PHENOMENOLOGY OF COSMIC RAY AIR SHOWERS

MARIA TERESA DOVA*

Departamento de Física,
Universidad Nacional de La Plata, CC67 La Plata (1900), Argentina
E-mail: dova@fisica.unlp.edu.ar

The properties of cosmic rays with energies above 10^6 GeV have to be deduced from the spacetime structure and particle content of the air showers which they initiate. In this review, a summary of the phenomenology of these giant air showers is presented. We describe the hadronic interaction models used to extrapolate results from collider data to ultra high energies, an also the main electromagnetic processes that govern the longitudinal shower evolution as well as the lateral spread of particles.

1. Introduction

For primary cosmic ray energies above 10^6 GeV, the flux becomes so low that direct detection of the primary particle using detectors in or above the upper atmosphere is not longer possible. In these cases the primary particle has enough energy to initiate an extensive air shower (EAS) in the atmosphere. If the primary cosmic ray particle is a nucleon or nucleus the cascade begins with a hadronic interaction. The number of hadrons increases through subsequent generations of particle interactions. In each generation about 20% of the energy is transferred to an electromagnetic cascade by rapid decays of neutral pions. Ultimately, the electromagnetic cascade dissipates roughly 90% of the primary particle's energy trough ionization. The remaining energy is carried by muons and neutrinos from charged pion decays. The electromagnetic and weak interactions are rather well understood. However, uncertainties in hadronic interactions at ultra high energies constitute one of the most problematic sources of systematic error in analysis of air showers. In what follows a brief report of the phenomenology of EAS is presented, focusing in those aspects which are the

*Work partially supported by CONICET, Argentina

main source of systematic uncertainties affecting somehow the determination of primary energy and mass composition. A complete review on the phenomenology of cosmic ray air showers can be found in [1].

2. Hadronic Processes

Soft multiparticle production with small transverse momenta with respect to the collision axis is a dominant feature of most hadronic events at center-of-mass energies 10 GeV $< \sqrt{s} <$ 50 GeV. Despite the fact that strict calculations based on ordinary QCD perturbation theory are not feasible, there are some phenomenological models that successfully take into account the main properties of the soft diffractive processes. These models, inspired by $1/N$ QCD expansion are also supplemented with generally accepted theoretical principles like duality, unitarity, Regge behavior, and parton structure. The interactions are no longer described by single particle exchange, but by highly complicated modes known as Reggeons. Up to about 50 GeV, the slow growth of the cross section with $\sqrt{s}$ is driven by a dominant contribution of a special Reggeon, the Pomeron.

At higher energies, semihard interactions arising from the hard scattering of partons that carry only a very small fraction of the momenta of their parent hadrons can compete successfully with soft processes. These semihard interactions lead to the minijet phenomenon, i.e., jets with transverse energy ($E_T = |p_T|$) much smaller than the total center-of-mass energy. Unlike soft processes, this low-p_T jet physics can be computed in perturbative QCD. The parton-parton minijet cross section is given by

$$\sigma_{\rm QCD}(s, p_T^{\rm cutoff}) = \sum_{i,j} \int \frac{dx_1}{x_1} \int \frac{dx_2}{x_2} \int_{Q^2_{\rm min}}^{\hat{s}/2} d|\hat{t}| \; \frac{d\hat{\sigma}_{ij}}{d|\hat{t}|} \; x_1 f_i(x_1, |\hat{t}|) \; x_2 f_j(x_2, |\hat{t}|) \;\; , \tag{1}$$

where x_1 and x_2 are the fractions of the momenta of the parent hadrons carried by the partons which collide, $d\hat{\sigma}_{ij}/d|\hat{t}|$ is the cross section for scattering of partons of types i and j according to elementary QCD diagrams, f_i and f_j are parton distribution functions (pdf's), $\hat{s} = x_1\, x_2 s$ and $-\hat{t} = \hat{s}\,(1 - \cos\vartheta^*)/2 = Q^2$ are the Mandelstam variables for this parton-parton process, and the sum is over all parton species. The integration limits satisfy $Q^2_{\rm min} < |\hat{t}| < \hat{s}/2$, with $Q_{\rm min}$ the minimal momentum transfer.

A first source of uncertainty in modeling cosmic ray interactions at ultra high energy is encoded in the extrapolation of the measured parton densities several orders of magnitude down to low x. Primary protons that

impact on the upper atmosphere with energy $\approx 10^{11}$ GeV, yield partons with $x \equiv 2p_{\parallel}^{*}/\sqrt{s} \approx m_{\pi}/\sqrt{s} \sim 10^{-7}$, whereas current data on quark and gluon densities are only available for $x \approx 10^{-4}$ to within an experimental accuracy of 3% for $Q^2 \approx 20$ GeV^2 [6]. Moreover, application of HERA data to baryonic cosmic rays assumes universality of the pdf's.

For large Q^2 and not too small x, the Dokshitzer-Gribov-Lipatov-Altarelli-Parisi (DGLAP) equations successfully predict the Q^2 dependence of the quark and gluon densities (q and g, respectively). In the double–leading–logarithmic approximation the DGLAP equations predict a steeply rising gluon density, $xg \sim x^{-0.4}$, which dominates the quark density at low x, in agreement with experimental results obtained with the HERA collider [7]. Specifically, HERA data are found to be consistent with a power law, $xg(x,Q^2) \sim x^{-\Delta_{\rm H}}$, with an exponent $\Delta_{\rm H}$ between 0.3 and 0.4 [8].

The high energy minijet cross section is then determined by the small-x behavior of the parton distributions or, rather, by that of the dominant gluon distribution (via the lower limits of the x_1, x_2 integrations) which gives [9]:

$$\sigma_{\rm QCD}(s) \propto \int_{2\,Q^2_{\rm min}/s}^{1} \frac{dx_1}{x_1}\, x_1^{-\Delta_{\rm H}} \int_{2\,Q^2_{\rm min}/s}^{1} \frac{dx_2}{x_2}\, x_2^{-\Delta_{\rm H}} \sim s^{\Delta_{\rm H}}\, \ln(s/s_0)\,, \quad (2)$$

where s_0 is a normalization constant. One caveat is that the inclusive QCD cross section given in Eq. (2) is a Born approximation, and therefore automatically violates unitarity.

The procedure of calculating the inelastic cross section from inclusive cross sections is known as unitarization. In the eikonal model [11] of high energy hadron-hadron scattering,the inelastic cross section, assuming a real eikonal function, is given by

$$\sigma_{\rm inel} = \int d^2\vec{b}\, \left\{1 - \exp\left[-2\chi_{\rm soft}(s,\vec{b}) - 2\chi_{\rm hard}(s,\vec{b})\right]\right\}\,, \quad (3)$$

where the scattering is compounded as a sum of QCD ladders via hard and soft processes through the eikonals $\chi_{\rm hard}$ and $\chi_{\rm soft}$. It should be noted that we have ignored spin-dependent effects and the small real part of the scattering amplitude, both good approximations at high energies. Now, if the eikonal function, $\chi(s,\vec{b}) \equiv \chi_{\rm soft}(s,\vec{b}) + \chi_{\rm hard}(s,\vec{b}) = \lambda/2$, indicates the mean number of partonic interaction pairs at impact parameter $\vec{b}$, the probability p_n for having n independent partonic interactions using Poisson statistics reads, $p_n = (\lambda^n/n!)\, e^{-\lambda}$. Therefore, the factor $1 - e^{-2\chi} = \sum_{n=1}^{\infty} p_n$ in Eq. (3) can be interpreted semiclassically as the probability that at least 1 of the 2 protons is broken up in a collision at impact parameter $\vec{b}$. With

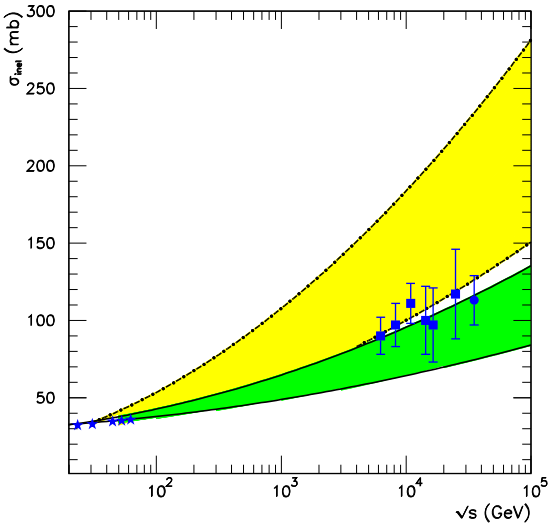

Figure 1. Energy dependence of the pp inelastic cross section as predicted by Eqs. (5) and (6) with $0.3 < \Delta_{\rm H} < 0.4$. The darkly shaded region between the solid lines corresponds to the model with Gaussian parton distribution in $\vec{b}$. The region between the dashed-dotted lines corresponds to the model with exponential fall-off of the parton density in $\vec{b}$.

this in mind, the inelastic cross section is simply the integral over all collision impact parameters of the probability of having at least 1 interaction, yielding a mean minijet multiplicity of $\langle n_{\rm jet}\rangle \approx \sigma_{\rm QCD}/\sigma_{\rm inel}$ [12]. The leading contenders to approximate the (unknown) cross sections at cosmic ray energies, SIBYLL [13] and QGSJET [14], share the eikonal approximation but differ in their *ansätse* for the eikonals. In both cases, the core of dominant scattering at very high energies is the parton-parton minijet cross section given in Eq. (1),

$$\chi_{\rm hard} = \frac{1}{2}\,\sigma_{\rm QCD}(s, p_T^{\rm cutoff})\; A(s,\vec{b})\,, \tag{4}$$

where the normalized profile function, $\int d^2\vec{b}\; A(s,\vec{b}) = 1$, indicates the distribution of partons in the plane transverse to the collision axis.

In the QGSJET-like models, the core of the hard eikonal is dressed with a soft-pomeron pre-evolution factor. This amounts to taking a parton distribution which is Gaussian in the transverse coordinate distance $|\vec{b}|$.

In SIBYLL-like models, the transverse density distribution is taken as the Fourier transform of the proton electric form factor, resulting in an energy-independent exponential (rather than Gaussian) fall-off of the par-

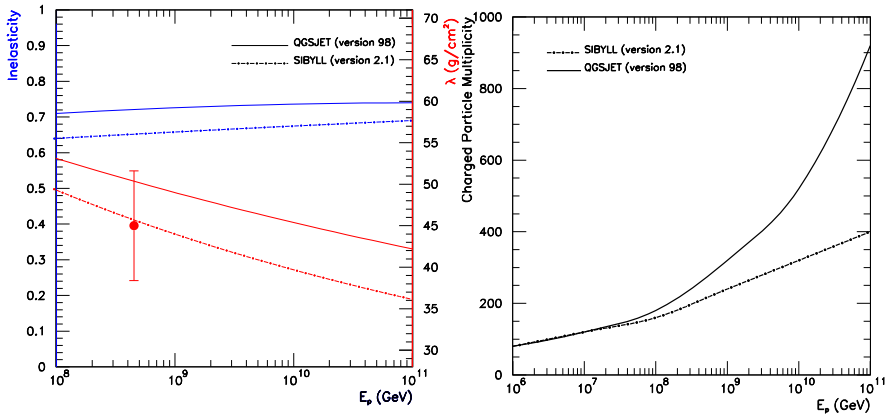

Figure 2. Left panel: The slowly rising curves indicate the mean inelasticity in proton air collisions as predicted by QGSJET and SIBYLL. The falling curves indicate the proton mean free path in the atmosphere. Right panel: Mean multiplicity of charged secondary particles produced in inelastic proton-air collisions processed with QGSJET and SIBYLL.

ton density profile with $|\vec{b}|$. The main characteristics of the pp cascade spectrum resulting from these choices are readily predictable: the harder form of the SIBYLL form factor allows a greater retention of energy by the leading particle, and hence less available for the ensuing shower. Consequently, on average SIBYLL-like models predict a smaller multiplicity than QGSJET-like models (see *e.g.* [16,17,18,19]).

At high energy, $\chi_{\rm soft} \ll \chi_{\rm hard}$, and so the inelastic cross section is dominated by the hard eikonal. With the appropriate choice of normalization, the cross section in Eq. (2) can be well–approximated by a power law. This implies that the growth of the inelastic cross section according to QGSJET-like models is given by

$$\sigma_{\rm inel} \sim \int d^2\vec{b}\ \Theta(b_s - |\vec{b}|) = \pi b_s^2 \sim 4\pi\, \alpha'_{\rm eff}\ \Delta_{\rm H}\ \ln^2(s/s_0) \sim 0.52\ \Delta_{\rm H}\ \ln^2(s/s_0)\ \ {\rm mb}\ . \tag{5}$$

For SIBYLL-like models, the growth of the inelastic cross section also saturates the $\ln^2 s$ Froissart bound, but with a multiplicative constant which is larger than the one in QGSJET-like models [18]. Namely,

$$\sigma_{\rm inel} \sim 3.2\ \Delta_{\rm H}^2 \ln^2(s/s_0)\ \ {\rm mb}\ . \tag{6}$$

Figure 1 illustrates the large range of predictions for pp inelastic cross section which remain consistent with HERA data. When the two leading order approximations discussed above are extrapolated to higher energies,

both are consistent with existing cosmic ray data. Note, however, that in both cases the range of allowed cross-sections at high energy varies by a factor of about 2 to 3. The points in Fig. 1 correspond to the most up-to-date estimate of the *pp* cross section from cosmic ray shower data [21].

There are three event generators, SIBYLL [13], QGSJET [14], and DPMJET [24] which are tailored specifically for simulation of hadronic interactions up to the highest cosmic ray energies. The latest versions of these packages are SIBYLL 2.1 [25], QGSJET 01 [26], and DPMJET III [27]; respectively. In QGSJET, both the soft and hard processes are formulated in terms of Pomeron exchanges. To describe the minijets, the soft Pomeron mutates into a "semi-hard Pomeron", an ordinary soft Pomeron with the middle piece replaced by a QCD parton ladder, as sketched in the previous paragraph. This is generally referred to as the "quasi-eikonal" model. In contrast, SIBYLL and DPMJET follow a "two channel" eikonal model, where the soft and the semi-hard regimes are demarcated by a sharp cut in the transverse momentum: SIBYLL 2.1 uses a cutoff parametrization inspired in the double leading logarithmic approximation of the DGLAP equations, whereas DPMJET III uses an *ad hoc* parametrization for the transverse momentum cutoff [8].

The transition process from asymptotically free partons to colour-neutral hadrons is described in all codes by string fragmentation models [28]. Different choices of fragmentation functions can lead to some differences in the hadron multiplicities. However, the main difference in the predictions of QGSJET-like and SIBYLL-like models arises from different assumptions in extrapolation of the parton distribution function to low energy.

Now we turn to nucleus-nucleus interactions, which cause additional headaches for event generators which must somehow extrapolate *pp* interactions in order to simulate the proton-air collisions of interest. All the event generators described above adopt the Glauber formalism [10].

Since the codes described above are still being refined, the disparity between them can vary even from version to version. At the end of the day, however, the relevant parameters boil down to two: the mean free path, $\lambda = (\widetilde{\sigma}_{\rm prod}\, n)^{-1}$, and the inelasticity, $K = 1 - E_{\rm lead}/E_{\rm proj}$, where n is the number density of atmospheric target nucleons, $E_{\rm lead}$ is the energy of the most energetic hadron with a long lifetime, and $E_{\rm proj}$ is the energy of the projectile particle. Overall, SIBYLL has a shorter mean free path and a smaller inelasticity than QGSJET, as indicated in Fig. 2. Since a shorter mean free path tends to compensate a smaller inelasticity, the two codes generate similar predictions for an air shower which has lived through several generations. The different predictions for the mean charged particle

multiplicity in proton-air collisions are shown in Fig. 2. Both models predict the same multiplicity below about 10^7 GeV, but the predictions diverge above that energy. Such a divergence readily increases with rising energy. As it is extremely difficult to observe the first interactions experimentally, it is not straightforward to determine which model is closer to reality.

3. Electromagnetic Component

The evolution of an extensive air shower is dominated by electromagnetic processes. The interaction of a baryonic cosmic ray with an air nucleus high in the atmosphere leads to a cascade of secondary mesons and nucleons. The first few generations of charged pions interact again, producing a hadronic core, which continues to feed the electromagnetic and muonic components of the showers. Up to about 50 km above sea level, the density of atmospheric target nucleons is $n \sim 10^{20}$ cm^{-3}, and so even for relatively low energies, say $E_{\pi^\pm} \approx 1$ TeV, the probability of decay before interaction falls below 10%. Ultimately, the electromagnetic cascade dissipates around 90% of the primary particle's energy, and hence the total number of electromagnetic particles is very nearly proportional to the shower energy.

By the time a vertically incident 10^{11} GeV proton shower reaches the ground, there are about 10^{11} secondaries with energy above 90 keV in the the annular region extending 8 m to 8 km from the shower core. Of these, 99% are photons, electrons, and positrons, with a typical ratio of γ to e^+e^- of 9 to 1. Their mean energy is around 10 MeV and they transport 85% of the total energy at ground level. Of course, photon-induced showers are even more dominated by the electromagnetic channel, as the only significant muon generation mechanism in this case is the decay of charged pions and kaons produced in γ-air interactions.

It is worth mentioning that these figures dramatically change for the case of very inclined showers. For a primary zenith angle, $\theta > 70^\circ$, the electromagnetic component becomes attenuated exponentially with atmospheric depth, being almost completely absorbed at ground level. We remind the reader that the vertical atmosphere is ≈ 1000 g/cm^2, and is about 36 times deeper for completely horizontal showers.

In contrast to hadronic collisions, the electromagnetic interactions of shower particles can be calculated very accurately from quantum electrodynamics. Electromagnetic interactions are thus not a major source of systematic errors in shower simulations. The first comprehensive treatment of electromagnetic showers was elaborated by Rossi and Greissen [29].

This treatment was recently cast in a more pedagogical form by Gaisser [30] and a summary is presented in [1].

The generation of the electromagnetic component is driven by electron bremsstrahlung and pair production [31]. Eventually the average energy per particle drops below a critical energy, ϵ_0, at which point ionization takes over from bremsstrahlung and pair production as the dominant energy loss mechanism. The $e^{\pm}$ energy loss rate due to bremsstrahlung radiation is nearly proportional to their energy, whereas the ionization loss rate varies only logarithmically with the $e^{\pm}$ energy. The changeover from radiation losses to ionization losses depopulates the shower. One can thus categorize the shower development in three phases: the growth phase, in which all the particles have energy $> \epsilon_0$; the shower maximum, $X_{\max}$; and the shower tail, where the particles only lose energy, get absorbed or decay.

The relevant quantities participating in the development of the electromagnetic cascade are the probability for an electron of energy E to radiate a photon of energy $k = yE$ and the probability for a photon to produce a pair e^+e^- in which one of the particles (hereafter e^-) has energy $E = xk$. These probabilities are determined by the properties of the air and the cross sections of the two processes.

In the energy range of interest, the impact parameter of the electron or photon is larger than an atomic radius, so the nuclear field is screened by its electron cloud. In the case of complete screening, where the momentum transfer is small, the cross section for bremsstrahlung can be approximated by [32]

$$\frac{d\sigma_{e\to\gamma}}{dk} \approx \frac{A_{\rm eff}}{X_0 N_A k}\left(\frac{4}{3} - \frac{4}{3}y + y^2\right) \ , \tag{7}$$

where $A_{\rm eff}$ is the effective mass number of the air, X_0 is a constant, and N_A is Avogadro's number. In the infrared limit (*i.e.*, $y \ll 1$) this approximation is inaccurate at the level of about 2.5%, which is small compared to typical experimental errors associated with cosmic air shower detectors. Of course, the approximation fails as $y \to 1$, when nuclear screening becomes incomplete, and as $y \to 0$, at which point the LPM and dielectric suppression effects become important.This infrared divergence is eliminated by the interference of bremsstrahlung amplitudes from multiple scattering centers. This collective effect of the electric potential of several atoms is known as the Landau-Pomeranchuk-Migdal (LPM) effect [33,34]. Using similar approximations, the cross section for pair production can be obtained [32].

The LPM suppression of the cross section results in an effective increase

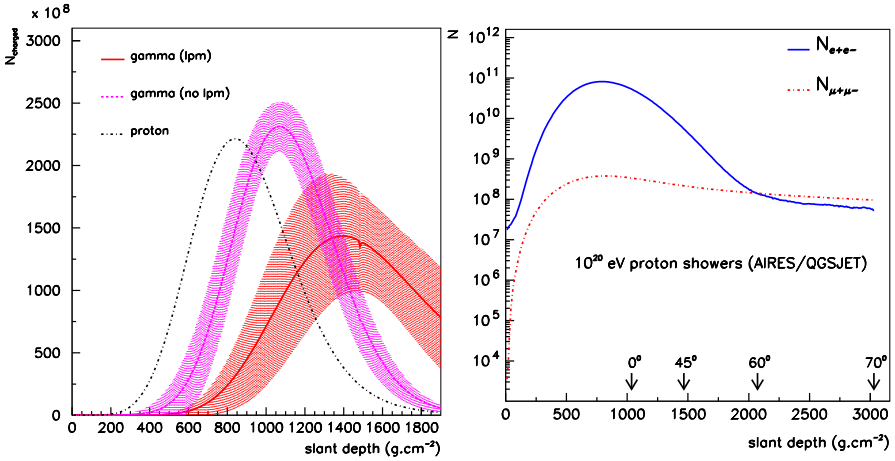

Figure 3. Left panel:Average longitudinal shower developments of 10^{11} GeV proton (dashed-dotted line) and γ-rays with and without the LPM effect (solid and dotted lines, respectively). The primary zenith angle was set to $\theta = 60°$. Right panel: Longitudinal development of muons and electrons as a function of the slant depth for 10^{11} GeV proton-induced showers.

of the mean free path of electrons and photons. This effectively retards the development of the electromagnetic component of the shower. It is natural to introduce an energy scale, $E_{\rm LPM}$, at which the inelasticity is low enough that the LPM effect becomes significant [35].

The experimental confirmation of the LPM effect at Stanford Linear Accelerator Center (SLAC) [36] has motivated new analyses of its consequences in cosmic ray physics [37,38,39,40]. The most evident signatures of the LPM effect on shower development are a shift in the position of the shower maximum $X_{\rm max}$ and larger fluctuations in the shower development.

Since the upper atmosphere is very thin the LPM effect becomes noticeable only for photons and electrons with energies above $E_{\rm LPM} \sim 10^{10}$ GeV. For baryonic primaries the LPM effect does not become important until the primary energy exceeds 10^{12}GeV. To give a visual impression of how the LPM effect slows down the initial growth of high energy photon-induced showers, we show the average longitudinal shower development of 10^{10} GeV proton and γ-ray showers (generated using AIRES 2.6.0 [41]) with and without the LPM effect in Fig. 3.

At energies at which the LPM effect is important (*viz.*, $E > E_{\rm LPM}$), γ-ray showers will have already commenced in the geomagnetic field at al-

most all latitudes. This reduces the energies of the primaries that reach the atmosphere, and thereby compensates the tendency of the LPM effect to retard the shower development. The first description of photon interactions in the geomagnetic field dates back at least as far as 1966 [42], with a punctuated revival of activity in the early 1980's [43]. More recently, a rekindling of interest in the topic has led to refined calculations [44,45]. Primary photons with energies above 10^{10} GeV convert into e^+e^- pairs, which in turn emit synchrotron photons. Regardless of the primary energy, the spectrum of the resulting photon "preshower" entering the upper atmosphere extends over several decades below the primary photon energy, and is peaked at energies below 10^{10} GeV [44]. The geomagnetic cooling thus switches on at about the same energy at which the LPM effect does, and thereby preempts the LPM-related observables which would otherwise be evident.

The relevant parameter to determine both conversion probability and synchrotron emission is $E \times B_\perp$, where E is the γ-ray energy and $B_\perp$ the transverse magnetic field. This leads to a large directional and geographical dependence of shower observables. Thus, each experiment has its own preferred direction for identifying primary gamma rays.

3.0.1. *Electron lateral distribution function*

The transverse development of electromagnetic showers is dominated by Coulomb scattering of charged particles off the nuclei in the atmosphere. The lateral development in electromagnetic cascades in different materials scales well with the Molière radius $r_{\rm M} = E_s\, X_0/\epsilon_0$, which varies inversely with the density of the medium,$r_{\rm M} = r_{\rm M}(h_{\rm OL})\ \frac{\rho_{\rm atm}(h_{\rm OL})}{\rho_{\rm atm}(h)} \simeq \frac{9.0\ {\rm g/cm^2}}{\rho_{\rm atm}(h)}$, where $E_s \approx 21$ MeV and the subscript OL indicates a quantity taken at a given observation level.

Approximate calculations of cascade equations in three dimensions to derive the lateral structure function for a pure electromagnetic cascade in vertical showers were obtained by Nishimura and Kamata [51], and later worked out by Greisen [52] in the well-known NKG formula,

$$\rho(r) = \frac{N_e}{r_{\rm M}^2}\, C\, \left(\frac{r}{r_{\rm M}}\right)^{s_{\rm NKG}-2} \left(1+\frac{r}{r_{\rm M}}\right)^{s_{\rm NKG}-4.5} \quad , \tag{8}$$

where N_e is the total number of electrons, r is the distance from the shower axis. For a primary of energy E_0, the so-called "age parameter", $s_{\rm NKG} = 3\,/(1+\frac{2\,\ln(E_0/\epsilon_0)}{t})$, characterizes the stage of the shower development in terms of the depth of the shower in radiation lengths, *i.e.*, $t = \int_z^\infty \rho_{\rm atm}(z)\ dz/X_0$.

The NKG formula may also be extended to describe showers initiated by baryons [53]. In such an extension, one finds a deviation of behavior of the Molière radius when using a value of the age parameter which is derived from theoretical predictions for pure electromagnetic cascades. It is possible to generalize the NKG formula for the electromagnetic component of baryon-induced showers by modifying the exponents in Eq. (8) [53]. The derived NKG formula provides a good description of the e^+e^- lateral distribution at all stages of shower development for values of r sufficiently far from the hadronic core. Fortunately, this is the experimentally interesting region, since typical ground arrays can only measure densities at $r > 100$ m from the shower axis, where detectors are not saturated. It should be mentioned that an NKG-like formula can be used to parametrize the total particle's density observed in baryon-induced showers [54].

In the case of inclined showers, one normally analyzes particle densities in the plane perpendicular to the shower axis. Simply projecting distributions measured at the ground into this plane is a reasonable approach for near-vertical showers, but is not sufficient for inclined showers. In the latter case, additionally asymmetry is introduced because of both unequal attenuation of the electromagnetic components arriving at the ground earlier than and later than the core [53]. Moreover, deflections on the geomagnetic field become important for showers inclined by more than about 70°.

In the framework of cascade theory, any effect coming from the influence of the atmosphere should be accounted as a function of the slant depth t [51]. Following this idea, a LDF valid at all zenith angles $\theta < 70°$ can be determined by considering

$$t'(\theta, \zeta) = t \, \sec\theta \, (1 + K \, \cos\zeta)^{-1} \, , \tag{9}$$

where ζ is the azimuthal angle in the shower plane, $K = K_0 \, \tan\theta$, and K_0 is a constant extracted from the fit [53,55]. Then, the particle lateral distributions for inclined showers $\rho(r, t')$ are given by the corresponding vertical LDF $\rho(r, t)$ but evaluated at slant depth $t'(\theta, \zeta)$ where the dependence on the azimuthal angle is evident.

For zenith angles $\theta > 70°$, the surviving electromagnetic component at ground is mainly due to muon decay and, to a much smaller extent, hadronic interactions, pair production and bremsstrahlung. As a result the lateral distribution follows that of the muon rather closely. In Fig. 3 the longitudinal development of the muon and electron components are shown. It is evident from the figure that for very inclined showers the electromagnetic development is due mostly to muon decay [57,56].

3.1. *The muon component*

The muonic component of EAS differs from the electromagnetic component for two main reasons. First, muons are generated through the decay of cooled charged pions, and thus the muon content is sensitive to the initial baryonic content of the primary particle. Furthermore, since there is no "muonic cascade", the number of muons reaching the ground is much smaller than the number of electrons. Specifically, there are about 5×10^8 muons above 10 MeV at ground level for a vertical 10^{11} GeV proton induced shower. Second, the muon has a much smaller cross section for radiation and pair production than the electron, and so the muonic component of EAS develops differently than does the electromagnetic component. The smaller multiple scattering suffered by muons leads to earlier arrival times at the ground for muons than for the electromagnetic component.

The ratio of electrons to muons depends strongly on the distance from the core; for example, the e^+e^- to $\mu^+\mu^-$ ratio for a 10^{11} GeV vertical proton shower varies from 17 to 1 at 200 m from the core to 1 to 1 at 2000 m. The ratio between the electromagnetic and muonic shower components behaves somewhat differently in the case of inclined showers. For zenith angles greater than 60°, the $e^+e^-/\mu^+\mu^-$ ratio remains roughly constant at a given distance from the core. As the zenith angle grows beyond 60°, this ratio decreases, until at $\theta = 75°$, it is 400 times smaller than for a vertical shower. Another difference between inclined and vertical showers is that the average muon energy at ground changes dramatically. For horizontal showers, the lower energy muons are filtered out by a combination of energy loss mechanisms and the finite muon lifetime: for vertical showers, the average muon energy is 1 GeV, while for horizontal showers it is about 2 orders of magnitude greater.

High energy muons lose energy through e^+e^- pair production, muon-nucleus interaction, bremsstrahlung, and knock-on electron (δ-ray) production [58]. The first three processes are discrete in the sense that they are characterized by high inelasticity and a large mean free path. On the other hand, because of its short mean free path and its small inelasticity, knock-on electron production can be considered a continuous process. The muon bremsstrahlung cross section is suppressed by a factor of $(m_e/m_\mu)^2$ with respect to electron bremsstrahlung, see Eq. (7). Since the radiation length for air is about 36.7 g/cm^2, and the vertical atmospheric depth is 1000 g/cm^2, muon bremsstrahlung is of negligible importance for vertical air shower development. Energy loss due to muon-nucleus interactions is

somewhat smaller than muon bremsstrahlung. Energy loss by pair production is slightly more important than bremsstrahlung at about 1 GeV, and becomes increasingly dominant with energy. Finally, knock-on electrons have a very small mean free path, but also a very small inelasticity, so that this contribution to the energy loss is comparable to that from the hard processes.

In addition to muon production through charged pion decay, photons can directly generate muon pairs, or produce hadron pairs which in turn decay to muons. In the case of direct pair production, the large muon mass leads to a higher threshold for this process than for electron pair production. Furthermore, QED predicts that $\mu^+\mu^-$ production is suppressed by a factor $(m_e/m_\mu)^2$ compared the Bethe-Heitler cross section. The cross section for hadron production by photons is much less certain, since it involves the *hadronic structure* of the photon. This has been measured at HERA for photon energies corresponding to $E_{\rm lab} = 2 \times 10^4$ GeV. This energy is still well below the energies of the highest energy cosmic rays, but nonetheless, these data do constrain the extrapolation of the cross sections to high energies.

The muon content of the shower tail is quite sensitive to unknown details of hadronic physics. This implies that attempts to extract composition information from measurements of muon content at ground level tend to be systematics dominated. The muon LDF is mostly determined by the distribution in phase space of the parent pions. However, the pionization process together with muon deflection in the geomagnetic field obscures the distribution of the first generation of pions. A combination of detailed simulations, high statistics measurements of the muon LDF and identification of the primary species using uncorrelated observables could shed light on hadronic interaction models.

Acknowledgments

I would like to thank the organizers for the financial support and warn hospitality. I am grateful to L. Anchordoqui, A. Mariazzi, T. McCauley, T. Paul, S. Reucroft and J Swain for providing a very productive and agreeable working atmosphere in order to write our review article.

References

1. L. Anchordoqui, M.T. Dova, A. Mariazzi, T. McCauley, T. Paul, S. Reucroft, J Swain. *Ann. Phys.*,**314**, 145 (2004) [arXiv:hep-ph/0407020]

2. A. Capella, U. Sukhatme, C. I. Tan and J. Tran Thanh Van, *Phys. Rept.* **236**, 225 (1994).
3. T. K. Gaisser and F. Halzen, *Phys. Rev. Lett.* **54**, 1754 (1985).
4. G. Pancheri and C. Rubbia, *Nucl. Phys. A* **418**, 117C (1984).
5. C. Albajar *et al.* [UA1 Collaboration], *Nucl. Phys. B* **309**, 405 (1988).
6. C. Adloff *et al.* [H1 Collaboration], *Eur. Phys. J. C* **21**, 33 (2001) [arXiv:hep-ex/0012053].
   Phys. Rev. D **59**, 074022 (1999) [arXiv:hep-ph/9805268].
7. H. Abramowicz and A. Caldwell, *Rev. Mod. Phys.* **71**, 1275 (1999) [arXiv:hep-ex/9903037].
8. R. Engel, *Nucl. Phys. Proc. Suppl.* **122**, 40 (2003).
9. J. Kwiecinski and A. D. Martin, *Phys. Rev. D* **43**, 1560 (1991).
10. R. J. Glauber and G. Matthiae, *Nucl. Phys. B* **21**, 135 (1970).
11. L. Durand and H. Pi, *Phys. Rev. D* **38**, 78 (1988).
12. T. K. Gaisser and T. Stanev, *Phys. Lett. B* **219**, 375 (1989).
13. R. S. Fletcher, T. K. Gaisser, P. Lipari and T. Stanev, *Phys. Rev. D* **50**, 5710 (1994).
14. N. N. Kalmykov, S. S. Ostapchenko and A. I. Pavlov, *Nucl. Phys. Proc. Suppl.* **52B**, 17 (1997).
15. F. Abe *et al.* [CDF Collaboration], *Phys. Rev. D* **56**, 3811 (1997).
16. L. A. Anchordoqui, M. T. Dova, L. N. Epele and S. J. Sciutto, *Phys. Rev. D* **59**, 094003 (1999) [arXiv:hep-ph/9810384].
17. L. A. Anchordoqui, M. T. Dova and S. J. Sciutto, Proc. 26th International Cosmic Ray Conference, Salt Lake City **1**, 147 (1999) [arXiv:hep-ph/9905248].
18. J. Alvarez-Muniz, R. Engel, T. K. Gaisser, J. A. Ortiz and T. Stanev, *Phys. Rev. D* **66**, 033011 (2002) [arXiv:astro-ph/0205302].
19. R. Engel and H. Rebel, *Acta Phys. Polon. B* **35**, 321 (2004).
20. U. Amaldi and K. R. Schubert, Nucl. Phys. B **166**, 301 (1980).
21. M. M. Block, F. Halzen and T. Stanev, *Phys. Rev. D* **62**, 077501 (2000) [arXiv:hep-ph/0004232].
22. M. Honda *et al.*, *Phys. Rev. Lett.* **70**, 525 (1993).
23. R. M. Baltrusaitis *et al.*, *Phys. Rev. Lett.* **52**, 1380 (1984).
24. J. Ranft, *Phys. Rev. D* **51**, 64 (1995).
25. R. Engel, T. K. Gaisser, T. Stanev and P. Lipari, Proc. 26th International Cosmic Ray Conference, Salt Lake City **1**, 415 (1999).
26. D. Heck, Proc. 27th International Cosmic Ray Conference, Hamburg, 233 (2001).
27. S. Roesler, R. Engel and J. Ranft, arXiv:hep-ph/0012252.
28. T. Sjostrand, *Int. J. Mod. Phys. A* **3**, 751 (1988).
29. B. Rossi and K. Greisen, *Rev. Mod. Phys.* **13**, 240 (1941).
30. T. K. Gaisser, *Cosmic Rays and Particle Physics,* (Cambridge University Press, 1990).
31. H. Bethe and W. Heitler, *Proc. Roy. Soc. Lond. A* **146**, 83 (1934).
32. Y. S. Tsai, *Rev. Mod. Phys.* **46**, 815 (1974) [Erratum *Rev. Mod. Phys.* **49**, 421 (1977)].
33. L. D. Landau and I. Pomeranchuk, *Dokl. Akad. Nauk Ser. Fiz.* **92**, 535 (1953).

34. A. B. Migdal, *Phys. Rev.* **103**, 1811 (1956).
35. T. Stanev, C. Vankov, R. E. Streitmatter, R. W. Ellsworth and T. Bowen, *Phys. Rev. D* **25**, 1291 (1982).
36. S. Klein, *Rev. Mod. Phys.* **71**, 1501 (1999) [arXiv:hep-ph/9802442].
37. J. Alvarez-Muniz and E. Zas, *Phys. Lett. B* **434**, 396 (1998) [arXiv:astro-ph/9806098].
38. A. N. Cillis, H. Fanchiotti, C. A. Garcia Canal and S. J. Sciutto, *Phys. Rev. D* **59**, 113012 (1999) [arXiv:astro-ph/9809334].
39. J. N. Capdevielle, C. Le Gall and K. N. Sanosian, *Astropart. Phys.* **13**, 259 (2000).
40. A. V. Plyasheshnikov and F. A. Aharonian, *J. Phys. G* **28**, 267 (2002) [arXiv:astro-ph/0107592].
41. S. J. Sciutto, arXiv:astro-ph/9911331.
42. T. Erber, *Rev. Mod. Phys.* **38**, 626 (1966).
43. B. Mcbreen and C. J. Lambert, *Phys. Rev. D* **24**, 2536 (1981).
44. X. Bertou, P. Billoir and S. Dagoret-Campagne, Astropart. Phys. **14**, 121 (2000).
45. P. Homola *et al.*, arXiv:astro-ph/0311442.
46. W. Heitler. *The Quantum Theory of Radiation*, 2nd. Edition, (Oxford University Press, London, 1944).
47. D. Heck, G. Schatz, T. Thouw, J. Knapp and J. N. Capdevielle, FZKA-6019 (1998).
48. J. Knapp, D. Heck, S. J. Sciutto, M. T. Dova and M. Risse, *Astropart. Phys.* **19**, 77 (2003) [arXiv:astro-ph/0206414].
49. H. J. Drescher and G. R. Farrar, *Phys. Rev. D* **67**, 116001 (2003) [arXiv:astro-ph/0212018].
50. H. J. Drescher and G. R. Farrar, *Astropart. Phys.* **19**, 235 (2003) [arXiv:hep-ph/0206112].
51. K. Kamata and J. Nishimura,*Progr. Theor. Phys. Suppl.* **6**, 93 (1958).
52. K. Greisen, *Ann. Rev. Nucl. Sci.* **10**, 63 (1960).
53. M. T. Dova, L. N. Epele and A. G. Mariazzi, *Astropart. Phys.* **18**, 351 (2003) [arXiv:astro-ph/0110237].
54. M. Roth [AUGER Collaboration], arXiv:astro-ph/0308392.
55. M. T. Dova, L. N. Epele and A. Mariazzi, *Nuovo Cim.* **24C**, 745 (2001).
56. A. Cillis and S. J. Sciutto, *J. Phys. G* **26**, 309 (2000).
57. M. Ave, R. A. Vazquez, E. Zas, J. A. Hinton and A. A. Watson, *Astropart. Phys.* **14**, 109 (2000) [arXiv:astro-ph/0003011].
58. A. N. Cillis and S. J. Sciutto, *Phys. Rev. D* **64**, 013010 (2001) [arXiv:astro-ph/0010488].